XL CILAMCE
IBERO-LATIN AMERICAN CONGRESS ON COMPUTATIONAL METHODS IN ENGINEERING
NOVEMBER 11-14, 2019
Praiamar Natal Hotel & Convention Natal, RN-BRAZIL

CROSS-SECTIONAL OPTIMAL DESIGN OF COLD-FORMED STEEL LIPPED CHANNELS USING ACCELERATED PARTICLE SWARM OPTIMIZATION

Felipe Ramos de Oliveira
João Alfredo de Lazzari
Eduardo de Miranda Batista
felipe.oliveira@coc.ufrj.br
joao.lazzari@coc.ufrj.br
batista@coc.ufrj.br
COPPE, Civil Engineering Program, Federal University of Rio de Janeiro
Centro de Tecnologia–Bloco I–Sala I216, Ilha do Fundão, CEP 21945-970, Rio de Janeiro/RJ, Brazil
Juarez Moara Santos Franco
juarezfranco@ufrrj.br
Instituto de Tecnologia, Universidade Federal Rural do Rio de Janeiro
Rodovia Br 465, Km 07, s/n - Zona Rural, Seropédica – RJ, Brazil

Abstract. This study aims to present a practical method for optimizing cold-formed steel (CFS) lipped channel beam-columns using an Accelerated Particle Swarm Optimization method (APSO). To eliminate impracticable cross-section shapes from the optimization results, several manufacturing and construction constraints are applied into the optimization process. Targeting this goal, 128 different lipped channel sections prototypes were selected and then optimized with respect to their buckling load, determined according to the finite strip method (FSM), then assessing the strength according to the provisions based on direct strength method (DSM). Comparing the structural resistance of the optimized sections with the sections of the original channel CFS with the same steel consumption, significant improvements were obtained. The results indicate that the optimized sections provide a compressive strength which is up to 50% higher than the initial shapes, and for flexural strength 30% higher than the reference profiles, while they meting predefined design and manufacturing constraints. The results of this study demonstrate the useful of APSO in CFS practical design problems.

Keywords: Cold-formed steel, Lipped Channel, Accelerated Particle Swarm Optimization, Direct Strength Method.

1 INTRODUCTION

Cold-formed steel (CFS) structural members are produced by bending thin metal sheets into a variety of cross-sectional shapes by either a cold-rolling or a press braking procedure, both performed at room temperature. They have several applications which are usually centered around their use in trusses, modular building panels, stud walls, purlins, side rails, cladding and even as the primary load-bearing structure in low- to mid-rise buildings. Normally, cold-rolling manufactories are able to custom roll sections on demand, adapted to specific applications. This flexible manufacturing system, makes the problem of maximizing material efficiency through selection of cross-sectional shapes a relevant topic to structural engineering [1].

While sections in current production by industry hold certain advantages in logistic/constructive practices, they may not be the most efficient in a structural perspective. On this regard, significant works have developed seeking more efficient cross sections using optimization algorithms. Initial efforts on the optimization of cold-formed steel members focused on optimizing the strength based on rules provided in specifications such as AISI [2], NBR 14762 [3], or Eurocode [4]. In particular, all of these specifications employ the effective width method for strength determination [5]. This design method affords a limited degree of generality and for best accuracy the basic cross-section typology (shape) must be pre-determined.

However, the Direct Strength Method (DSM), adopted by NBR 14762 in Appendix C [3], provides an analytical formulation capable to calculate the nominal load for diverse geometries of beam-columns, calibrated based on the appropriate categorization of the failure modes into the three buckling mode classes. The DSM applicability in arbitrary cross-sections favors the automatic strength computation of cold formed profiles, thus the development of optimization tools. In this work we used the open source software entitle FStr, developed in MATLAB by Thin Walled research group of the Federal University of Rio de Janeiro (COPPE-UFRJ), which employs the Finite Strip Method (FSM), for finding L, D and G buckling modes and load factors, respectively local (L), distortional (D) and global-Euler or flexural-torsional buckling (G).

The CFS cross section optimization algorithms may progress based on gradient method programming, or based on principles of stochastic search. The first one is capable of identifying local optimum but are restricted to problems where design sensitivities, or derivatives of performance metrics with respect to cross section design variables, are available. On the other hand, stochastic search algorithms do not require sensitivity information and thus may be applied to discrete problems, such as optimizing cross section selected from a database. The disadvantages are that they are heuristic trial-and-error methods, requiring a large number of analyses with no guarantee that an optimal solution will be found. In this paper the stochastic bio-inspired Accelerated Particle Swarm Optimization (APSO) algorithm was applied to maximize strength of cold-formed steel lipped channel profiles [6].

Several research projects have previously been carried out aimed at optimizing the relative dimensions of predefined conventional CFS cross-sections such as C, Z, or sigma– shapes. Near to the thematic of present paper, Ye et al. [7], [8] and Parastesh [9], using Particle Swarm Optimization (PSO) developed methodology using a combination of the Finite Strip Method (FSM) and the effective width method to optimize CFS beams-columns dimensions, considering conventional C– and sigma– variants, cross-sections.

The research presented in this paper aimed explore the performance of a family of cold-formed steel shapes constituted by 128 structural lipped channels elected from currently available industry sections. These CSF profiles are investigated in terms of their strength, given by the DSM, under axial uniform load and major-axis pure bending to establish the practical range of demands to be studied. Then, optimized them through APSO seeking for the best performance of lipped channel for a of axial and bending demand, for constants amounts of material. Given constraints imposed by NBR 14762, manufacturing limitations and practical considerations.

2 DESIGN OF CFS MEMBERS BASED ON NBR 14762

2.1. Compressive strength

The calculation of the member strength follows the Direct Strength Method (DSM) adopted by NBR 14762 [3]. DSM determines the nominal compressive strength P_n, assuming P_n the lowest value between P_{ne}, P_{nl} and P_{nd}, of CFS columns provided the user specifies the yield load P_y and the elastic critical loads in global P_{cre}, local P_{crl} and distortional P_{crd} and buckling modes. Because the steel sheet width b and thickness t are fixed in each combination analysis, the cross-section area A and the yield load ($P_y = A \cdot F_y$) remain unchanged each combination. The finite strip method software FStr was applied to determine the critical load values P_{crl}, P_{crd}, and P_{cre}.

The nominal compressive strength in global buckling is given by:

$$P_{ne} = \left(0.658^{\lambda_0^2}\right) \cdot P_y \qquad for\ \lambda_0 \leq 1.5 \tag{1.a}$$

$$P_{ne} = \left(\frac{0.877}{\lambda_0^2}\right) \cdot P_y \qquad for\ \lambda_0 > 1.5 \tag{1.b}$$

where λ_0 is the global buckling slenderness, given by:

$$\lambda_0 = \left(\frac{P_y}{P_{cre}}\right)^{0.5}. \tag{2}$$

Because the local failure of compressed members might occur in combination with global buckling, DSM prescribes the calculation of the nominal strength of columns failing in local-global modes. The nominal strength for local-global buckling failure is given by:

$$P_{nl} = P_{ne} \qquad for\ \lambda_l \leq 0.776 \tag{3.a}$$

$$P_{nl} = \left(1 - \frac{0.15}{\lambda_l^{0.8}}\right) \cdot \frac{P_{ne}}{\lambda_l^{0.8}} \qquad for\ \lambda_l > 0.776 \tag{3.b}$$

where λ_l is the local-global buckling slenderness, given by:

$$\lambda_l = \left(\frac{P_{ne}}{P_{crl}}\right)^{0.5}. \tag{4}$$

Note that the global strength P_{ne} must always be calculated prior to local-global buckling strength P_{nl}. Additionally, the L-G strength P_{nle} was always considered in these calculations because $P_{ne} \leq P_{nle}$. The nominal strength for distortional buckling is given by:

$$P_{nd} = P_y \qquad for\ \lambda_d \leq 0.561 \tag{5.a}$$

$$P_{nd} = \left(1 - \frac{0.25}{\lambda_d^{1.2}}\right) \cdot \frac{P_y}{\lambda_d^{1.2}} \qquad for\ \lambda_d > 0.561 \tag{5.b}$$

where λ_d is the distortional buckling slenderness, given by:

$$\lambda_d = \left(\frac{P_y}{P_{crd}}\right)^{0.5}. \tag{6}$$

2.2. Flexural strength

The DSM determines the nominal flexural strength M_n , assuming M_n the lowest value between M_{ne}, M_{nl} and M_{nd}, of CFS beams, subjected to simple bending, provided the user specifies yield moment W_y ($W_y = W \cdot F_y$) and the elastic critical loads in local M_{crl}, distortional M_{crd} and global M_{cre} buckling modes. The finite strip method software FStr was employed to determine the critical load values M_{crl}, M_{crd}, and M_{cre}.

The nominal strength in the lateral torsional buckling is given by:

$$M_{ne} = W_y \qquad for\ \lambda_0 \leq 0.6 \tag{7.a}$$

$$M_{ne} = 1.11 \cdot \left(1 - 0.278^{\lambda_0^2}\right) \cdot W \cdot F_y \qquad for\ 0.6 < \lambda_0 < 1.336 \tag{7.b}$$

$$M_{ne} = \frac{W_y}{\lambda_0^2} \qquad for\ \lambda_0 \geq 1.336 \tag{7.c}$$

where λ_0 is the global buckling slenderness, given by:

$$\lambda_0 = \left(\frac{W_y}{P_{cre}}\right)^{0.5}. \tag{8}$$

Because the local failure of flexed members might occur in combination with lateral torsional buckling, DSM prescribes the calculation of the nominal strength of beams failing in local-global modes. The nominal strength for local-global buckling failure is given by:

$$M_{nl} = M_{ne} \qquad for\ \lambda_l \leq 0.776 \tag{9.a}$$

$$M_{nl} = \left(1 - \frac{0.15}{\lambda_l^{0.8}}\right) \cdot \frac{M_{ne}}{\lambda_l^{0.8}} \qquad for\ \lambda_l > 0.776 \tag{9.b}$$

where λ_l is the local-global buckling slenderness, given by:

$$\lambda_l = \left(\frac{M_{ne}}{M_{crl}}\right)^{0.5}. \tag{10}$$

The nominal strength for distortional buckling is given by:

$$M_{nd} = W_y \qquad for\ \lambda_d \leq 0.673 \tag{11.a}$$

$$M_{nd} = \left(1 - \frac{0.22}{\lambda_d}\right) \cdot \frac{W_y}{\lambda_d} \qquad for\ \lambda_d > 0.673 \tag{11.b}$$

where λ_d is the distortional buckling slenderness, given by:

$$\lambda_d = \left(\frac{W_y}{M_{crd}}\right)^{0.5}. \tag{12}$$

3 DEFINITION OF OPTIMIZATION PROBLEM

The optimization problem can be mathematically formulated as follows:

$$maximize: \quad f(x_1, x_2, x_3 \ldots x_d) = P_n \;\; or \;\; f(x_1, x_2, x_3 \ldots x_d) = M_n \tag{13}$$

where P_n and M_n , nominal compressive strength flexural and nominal flexural strength, respectively, are the objective functions. Throughout the optimization process two yield strengths f_y values was taken ($f_y = 345\ MPa$, $f_y = 410\ MPa$) , the Young's E modulus was kept constant at $210\ GPa$.

The design variables are represented as follows: $x_1 = b_w$, $x_2 = b_f$, $x_3 = b_s$, $x_4 = \phi$, where b_w, b_f and b_s represent web length, flange length and lip length, respectively, as Fig. 1 illustrates.

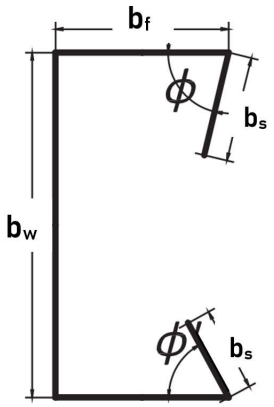

Figure 1. Lipped-channel's design variables

For each design variable x_i, lower and upper bounds were determined based on a combination of the constraints imposed by NBR 14762 and certain manufacturing limitations and practical considerations, which will be explained further in this section. Throughout the optimization process, eight cross-sections thickness t_c was taken ($t_c = 1.50\ mm$, $t_c = 2.00\ mm$, $t_c = 2.25\ mm$, $t_c = 2.65\ mm$, $t_c = 3.00\ mm$, $t_c = 3.25\ mm$, $t_c = 3.75\ mm$, $t_c = 3.75\ mm$) and eight total developed length of the cross-section (the coil width) L_f was taken ($L_f = 120\ mm$, $L_f = 200\ mm$, $L_f = 250\ mm$, $L_f = 300\ mm$, $L_f = 350\ mm$, $L_f = 400\ mm$, $L_f = 450\ mm$, $t_c = 500\ mm$). These values were taken from a commercially available channel section.

The optimization problem is bounded the following constraints:

$$0.10 \leq b_s/b_w \leq 0.30, \tag{14.a}$$
$$0.25 \leq b_f/b_w \leq 1.00, \tag{14.b}$$
$$0.25 \leq b_s/b_f \leq 0.60\ . \tag{14.c}$$

The lower and upper bounds are given by following equations:

$$50\ mm \leq b_w \leq 0.90 \cdot L_f, \tag{15.a}$$
$$30\ mm \leq b_f \leq 0.75 \cdot (L_f/2), \tag{15.b}$$
$$10\ mm \leq b_s \leq 0.25 \cdot (L_f/2). \tag{15.c}$$

Combining all f_y, t_c , L_f, values, this work prosed to optimize 128 different sets of domains to cold-formed steel lipped channel prototypes. In the calculus of nominal compressive strength and nominal flexural strength, was assumed beam-columns length L=1000 mm, simply supported, in both cases.

To ensure that the optimization process resulted in practically useful cross-sections, the following measures were taken. The basic overall shape of the cross-section was restricted to a lipped channel. In current construction practice, channels are the most commonly used CFS beam sections. The succession of flat plate elements within the cross-section permits a straightforward manufacturing process and allows for easy connections with trapezoidal steel deck or other roof/floor systems, as well as bridging, cleat plates, etc. This stands in contrast with the often complex and curved shapes typically encountered as the result of unrestricted shape optimization procedures. All prototypes are based on a traditional lipped channel shape typically within the capability of commercial cold-rolling enterprises. Each prototype was optimized individually, after which the overall optimum among the 128 optimized prototypes was identified.

In practical situations, additional constraints come out. These constraints may be quite case-dependent and may, for instance, be related to the ability to connect the beam-columns to other elements, or be imposed by the manufacturing process itself. In this particular case the following constraints were imposed:

a. The width of the flanges was required to be at least $30\ mm$ in order to connect trapezoidal decking or plywood boards to the beam by means of screws. This width was based on industrial practices;
b. The lip needs to be of a sufficient length. A lip of, for instance, 1 mm length cannot be rolled or brake-pressed. The industrial project practice suggested a minimum length of 5–10 mm. Therefore, as indicated in Eq. (15.c), $b_s \geq 10\ mm$ was imposed for a single lip;
c. The height of the web was specified to be at least $50\ mm$ in order to allow a connection to be made (e.g. to a cleat plate) with at least two bolts and/or for bridging to be connected;
d. The cross-sections must be symmetrical and lip's opening angles ϕ was fixed in $\pi/2$.

One of the major advantages of the PSO algorithm is that these constraints can easily be altered and others added. The constraints merely result in a restriction of the search space of the particle swarm.

In addition to the practical constraints mentioned above, the NBR 14762 design rules also impose certain limits on the plate width-to-thickness ratios, the relative dimensions of the cross-section and the angle of the edge stiffeners. These constraints were also taken into account in the optimization procedure.

The prototype's fundamental shape and the addition of practical constraints significantly restrict the solution space. An unconstrained 'free-form' optimization would most likely result in a cross-section with a higher ultimate capacity, with this 'overall optimum' solution not being contained within the current restricted search space. However, the aim of the research was to produce cross-sections with practical relevance.

4 PARTICLE SWARM OPTIMIZATION

Particle swarm optimization (PSO) was developed by Kennedy and Eberhart in 1995 based on swarms founded in nature, such as bird flock and fish shoal. Since then, PSO has generated much wider interests and forms an exciting, ever-expanding research subject, called swarm intelligence. PSO has been applied to almost every area in optimization, computational intelligence, and design applications. There are at least two dozen PSO variants, and hybrid algorithms by combining PSO with other existing algorithms are also investigated extensively [10].

4.1 Swarm Intelligence

The Swarm intelligence is an artificial intelligence (AI) field which studies the behavior of decentralized and self-organized systems, understanding by self-organization the ability of some physical systems formed by many individuals, to create behavior patterns adaptable and not predictable, without a central intelligence. Observing social organizations found in nature, as well as the behavioral characteristics of their colonies, inspires many swarm intelligence algorithms such as Ant Colony

Optimization (ACO) and Firefly Optimization Algorithm (FOA), e.g.

The PSO become one of the most popular swarm-intelligence-based algorithms due to its programming simplicity and flexibility face of several problems. Instead of using mutation and crossover, techniques applied in Genetic Algorithms (GA), PSO uses real-numbers randomness and collective communication between particles. Thus, there is no decoding of the parameters in binary numbers such as those present in AG.

Many new algorithms that are based on swarm intelligence may have drawn inspiration from different sources, but they have some similarity to some of the components that are used in PSO. In this sense, PSO pioneered the basic ideas of swarm-intelligence based computation [11].

4.2 PSO algorithm

The PSO algorithm consists in particle sets with n individuals, where each is random positioned within a parameters space (limiting a feasible region), each representing a possible solution of proposed problem. Each particle has velocity v which changes its position through the feasible region using a series of discrete timesteps t (iterations), in this work the PSO main algorithm was implemented in MATLAB. The velocity vector v for each particle is adjusted at each timestep t according to the best individual performance of that specific particle, as well as best performance of the swarm as a whole. The performance of each new candidate solution is quantified using an objective function, and the process is repeated until the convergence criteria are met. In this work, was adopt a swarm size $n = 20$ and a maximum iteration $t_{max} = 500$.

The potential solutions are represented by a vector x, which comprises a specific parameter set entering the possible solutions of a problem within a feasible region. In the PSO, the vector x represents a particle position. The particular particle position i at each timestep t is given by x_t^i and the velocity of particle i at each timestep t is given by v_t^i. The objective function $f(x)$ determines the performance of the position of each particle, the best value of objective function of any particle in the swarm at time t is given by f_t^i ,the historical best value of objective function in the swarm particle i until the time t is given by f_t^g. The global best position of any particle in the swarm at time t is given by P_t^i, while the historical best position in the swarm particle i until the time t is given by P_t^g.

The velocity of each particle is updated at each timestep according to Eq. (16), following:

$$v_{t+1}^i = w \cdot v_t^i + C_1 \cdot n_{r1} \cdot \left(P_t^i - x_t^i\right) + C_2 \cdot n_{r2} \cdot \left(P_t^g - x_t^i\right) \tag{16}$$

where n_{r1} and n_{r2} are random numbers from a Gaussian distribution with values between 0 to 1, C_1 and C_2 are cognitive acceleration factor and the social acceleration factor, respectively, and w is the inertia factor. These weighting factors are bounded according to the rules of Eq. (17) for algorithm convergence.

$$0 < (C_1 + C_2) < 4 \tag{17.a}$$

$$\frac{(C_1 + C_2)}{2} - 1 < w < 1\,. \tag{17.b}$$

The inertia term w, determines how much of the speed from the previous timestep is over to the next one. High inertia values cause particles to behave more independently and explore the solution space more meticulously, while lower values cause faster swarm convergence. One popular strategy for selecting the inertia term is to use a dynamic factor that begins at high value, and gradually decreases during algorithm interactions. This approach brings with it the advantage of a timely convergence while to force the particles to fully explore the solution space [12].

The cognitive acceleration factor C_1 (also known as the cognitive factor), multiplied by a random number $n_{r1} \in [0,1]$, determines the influence of the best historical performance of each individual particle. The social acceleration factor C_2 (also known as the swarm factor) multiplied by a random number $n_{r2} \in [0,1]$, determines the influence of the best historical performance of swarm. A high social acceleration factor value causes a quicker algorithm convergence to the best swarm position, but limits individual particle exploration. On the other hand, a high self-confidence parameter causes each particle

to fully explore any optimal regions each particle encounters, but may delay convergence. It is common for the cognitive acceleration factor to be equal to or slightly larger than the swarm influence parameter (in the range of 1.5 to 2.5), due to the convergence criteria in Eq. (17) leads to the best behavior of the PSO algorithm.

The essence steps of optimization algorithm through particle examination can be summarized in the pseudocode shown in Fig. 2.

PARTICLE SARW OPTIMIZATION

1: Objective function $\boldsymbol{f(x)}$, $\boldsymbol{x = (x_1, x_1, x_1 \ldots\ x_d)^T}$
2: Initialize locations $\boldsymbol{x_i}$ and velocity $\boldsymbol{v_i}$ of $\boldsymbol{n}$ particles
3: Finding $\boldsymbol{P_i^g}$ from min $\{f(x_1), f(x_2), f(x_3) \ldots . f(x_n)\}$ at $\boldsymbol{t = 0}$
4: ***while*** (criterion)
5: ***for*** loop over all $\boldsymbol{n}$ particles and **all** d dimensions
6: Calculate new velocity $\boldsymbol{v_{t+1}^i = w \cdot v_t^i + C_1 \cdot n_{r1} \cdot \left(P_t^i - x_t^i\right) + C_2 \cdot n_{r2} \cdot \left(P_t^g - x_t^i\right)}$
7: Calculate new locations $\boldsymbol{x_{t+1}^i = x_t^i + v_{t+1}^i}$
8: Evaluate objective functions at new locations $\boldsymbol{x_t^{i+1}}$
9: ***end for***
10: Find the current global best $\boldsymbol{P_t^i}$
11: Update $\boldsymbol{t = t + 1}$ (pseudo time or iteration counter)
11: ***end while***
12: Output the final results $\boldsymbol{f_t^g}$ and $\boldsymbol{P_i^g}$

Figure 2. PSO pseudocode [13]

4.3 Accelerated PSO

The standard PSO uses both best the current global best and the individual best. Using the individual best mostly to increase the diversity in the quality solutions. But this diversity can be simulated using some randomness. Thus, there is no compelling reason for using the individual best unless the optimization problem of interest is highly nonlinear and multimodal [13].

A simplified PSO version which uses only the global best to accelerates algorithm's convergence, is called of Accelerated Particle Swarm Optimization (APSO), its velocity vector is given by:

$$v_{t+1}^i = v_t^i + C_1 \cdot (n_r - 1/2) + C_2 \cdot \left(P_t^g - x_t^i\right) \tag{18}$$

where n_r is a random variable with values from 0 to 1. Here the shift 1/2 is purely out of convenience. We can also use a standard normal distribution $C_1 \cdot n_{rt}$, where n_{rt} is drawn from N (0, 1) to replace the second term. Now we have

$$v_{t+1}^i = v_t^i + C_2 \cdot \left(P_t^g - x_t^i\right) + C_1 \cdot n_{rt} \tag{19}$$

where n_{rt} can be drawn from a Gaussian distribution or any other suitable distributions. The update of the position is simply

$$x_{t+1}^i = x_t^i + v_{t+1}^i. \tag{20}$$

We can also simplify the formulation writing the update of the location in a single step

$$x_{t+1}^i = (1 - C_2) \cdot x_t^i + C_2 \cdot P_t^g + C_1 \cdot n_{rt}. \tag{21}$$

The typical initial values for the PSO are $C_1 \approx 0.2$ and $C_2 \approx 0.5$, for unimodal objective functions.

It is worth pointing out that the parameters C_1 and C_2 should in general be related to the scales of the independent variables x_t^i and the search domain.

In addition, the APSO brings an improvement reducing the randomness as interaction process proceeds. Usually using a monotonically decreasing function such as:

$$C_1 = C_0 \cdot \gamma^t \tag{22}$$

where $C_0 \approx 0.5{\sim}1.0$ is the initial value of the randomness parameter. Here t is the timesteps number, $0 < \gamma < 1$ is a control parameter. In this work, was adopt $\gamma = 0.9$.

5 RESULTS AND DISCUSSION

5.1. Compressive strength

Overall, the mean strength increase was 19.04%. The lowest strength increment was 0.09%, which indicates that some standard profiles already are close to the best performance. On the other hand, the largest difference was 50.36%, which suggests a reasonable possibility of improvement of some prototypes. The Fig. 3 shows results obtained by the APSO process.

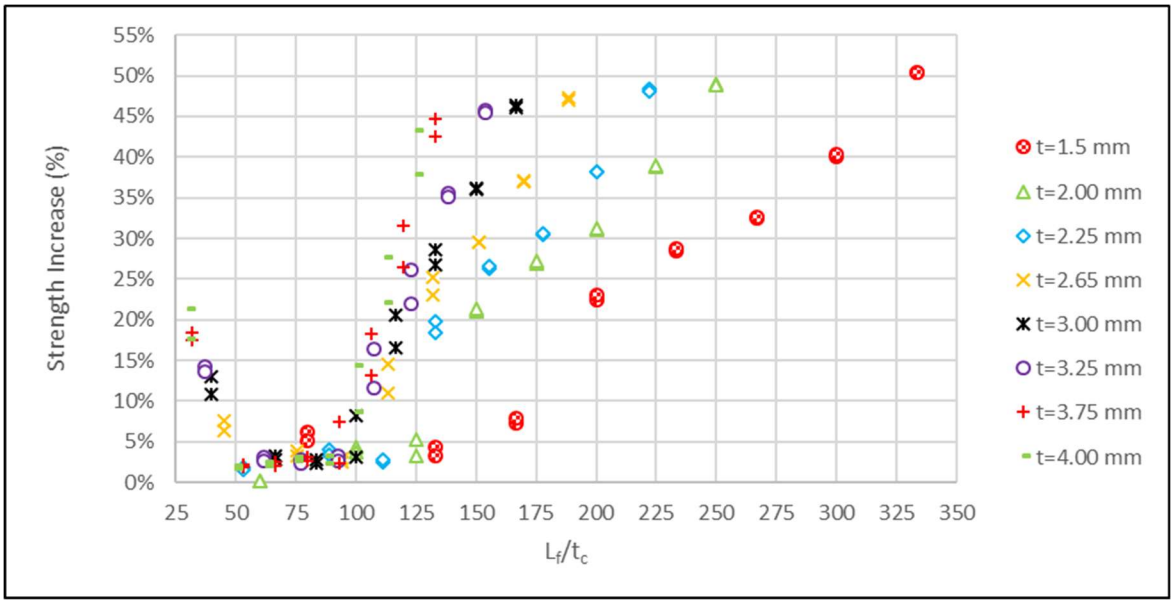

Figure 3. Compressive strength optimization results

Table 1 summarize the general results obtained by the APSO process.

Table 1. Descriptive Statistics over all compressive strength optimization

Descriptive Statistics	P_n (Increase)	b_f/b_w (Modification)	b_s/b_w (Modification)
Mean	19.04%	70.05%	111.88%
Standard Deviation	15.83%	84.90%	80.64%
Minimum	0.09%	-19.23%	13.64%
Maximum	50.36%	239.84%	248.00%

The mean b_f/b_w ratio was 0.65, which corresponds to 65% of imposed upper bound (Eq. (14.b)), and mean b_s/b_w was 0.29, which corresponds to 96.67% of imposed upper bound (Eq. (14.a)). Is noted

a high value of standard deviation of nominal strength indicating a variance in the optimization process, this fact is attributed to a greater or lesser proximity of some standard profiles of the best performance. It's worth pointing out that the b_s/b_w ratio of optimized profiles indicates there were lip's underutilization in all adopted protypes.

The results indicate great influence of local buckling and distortional buckling in the optimization problem, which was expected given the trend the of short beam-columns, as adopted in this work (L=1000 mm), to distance of Euler's buckling. The high shape variation rate is attributed to the negligible influence of the global buckling in these profiles, which makes the prototypes, basically subject to L and D buckling modes which are fundamentally governed by the cross-section geometry and sub-elements slender.

Table 2 presents the features of prototype with the lowest strength increment.

Table 2. Lowest compressive strength increment

Profile	f_y (MP_a)	L_f (mm)	t (mm)	P_n (kN)	b_w (mm)	b_f (mm)	b_s (mm)	b_f/b_w	b_s/b_w
Standard	410.00	120.00	2.00	42.90	50.00	25.00	10.00	0.50	0.20
Optimized	410.00	120.00	2.00	42.94	48.00	24.00	12.00	0.50	0.25

Table 3 presents the features of prototype with the greatest strength increment.

Table 3. Greatest compressive strength increment

Profile	f_y (MP_a)	L_f (mm)	t (mm)	P_n (kN)	b_w (mm)	b_f (mm)	b_s (mm)	b_f/b_w	b_s/b_w
Standard	345.000	500.00	2.00	143.08	290.00	80.00	25.00	0.28	0.09
Optimized	345.000	500.00	2.00	212.97	144.00	135.00	43.00	0.94	0.30

Figure 4 presents the shape modification of the prototype with the greatest strength increment.

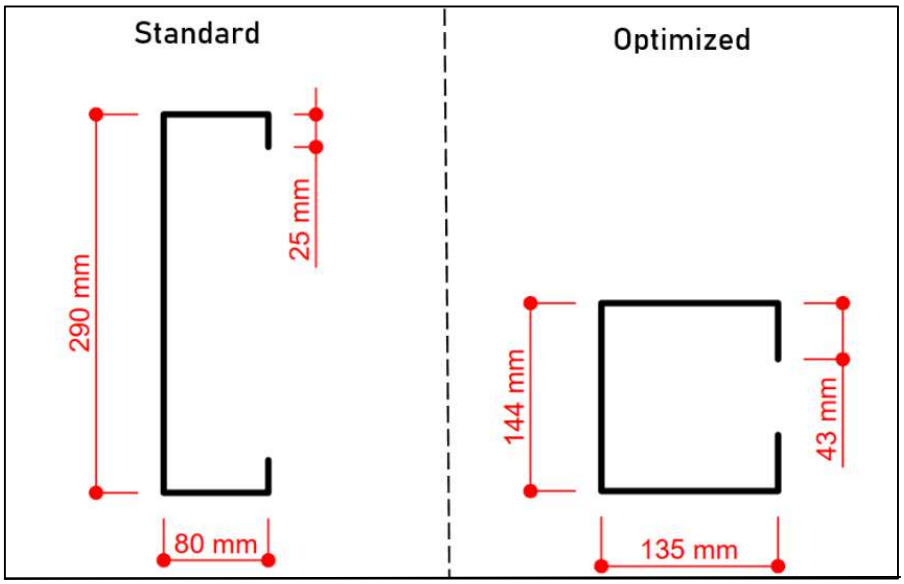

Figure 4. Shape modification of compressive strength optimization

The results in Figure 5 indicate that profiles manufactured from larger coils are more susceptible to optimization. This fact is related to the trend of the larger sub elements, which composes these

profiles, has in develop the L and D due to λ_l and λ_d increase.

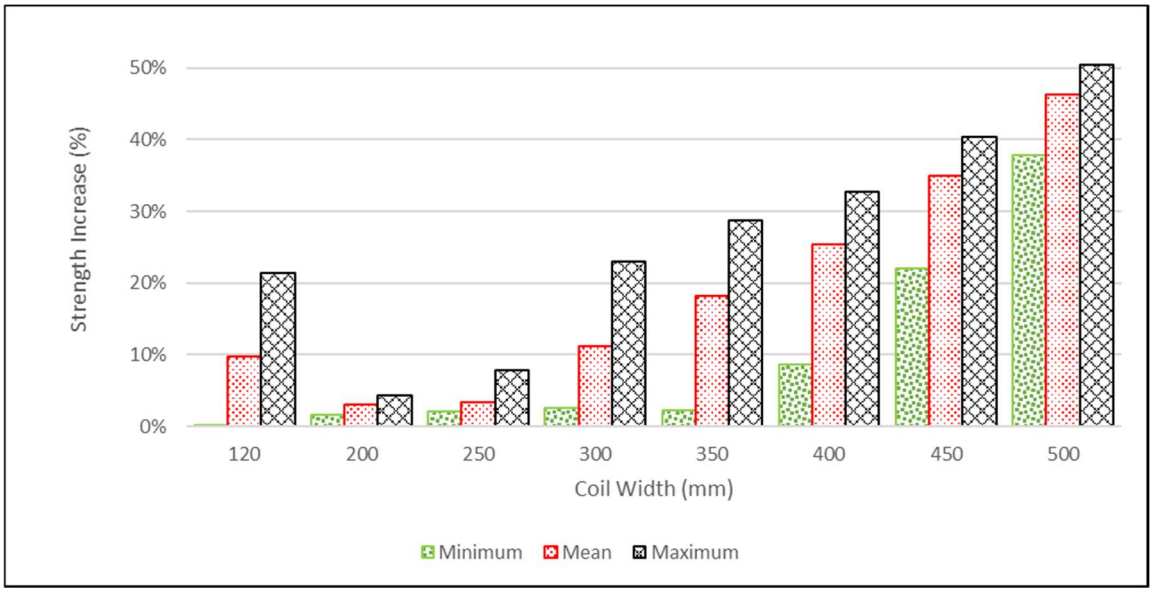

Figure 5. Compressive strength increase per coil width

The results in Figure 6 indicate that profiles manufactured from thinner coils are more susceptible to optimization. This fact is related to natural trend of slender sub-elements has in develop the L and D.

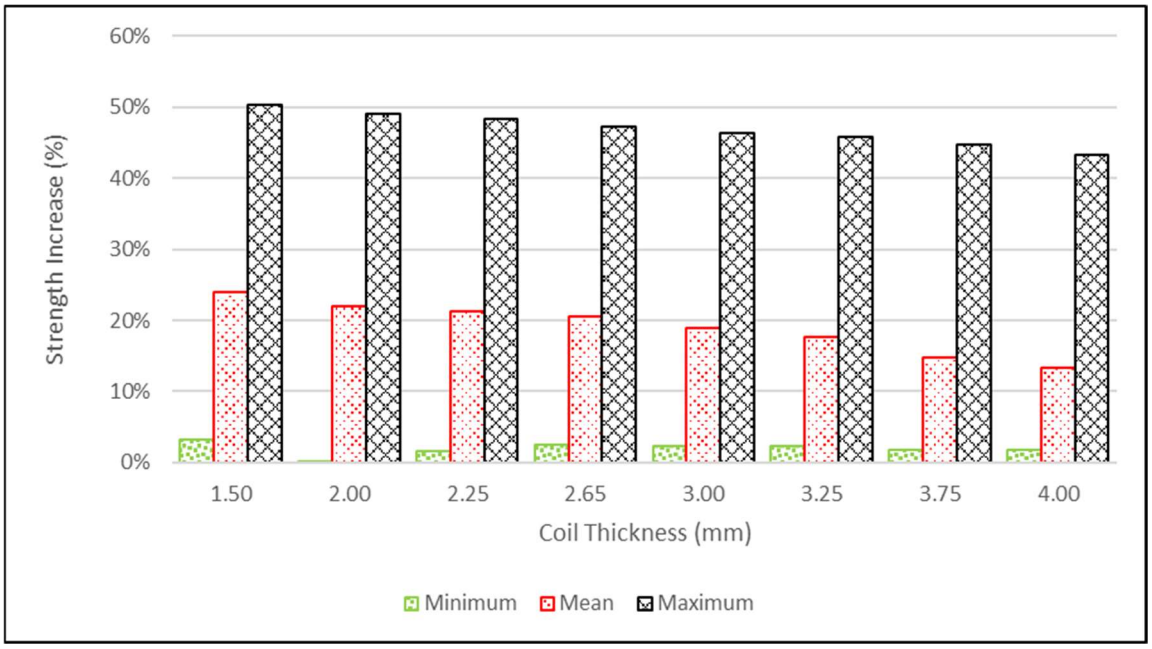

Figure 6. Compressive strength increase per coil thickness

The results indicate a possible L-D interaction, which would result in strength erosion not predicted by NBR 17642 even I the DSM formulation.

5.2. Flexural strength

Considering all protypes, the mean strength increase was 14.08%. One prototype could not be optimized, and the largest strength increase was 33.33%. The results indicate that, compared to the results observed in the compressive strength the APSO achieved a worse performance for flexural

strength, possibly due to the complex nature of the problem of flexional buckling. The Fig. 7 shows results obtained by the APSO process.

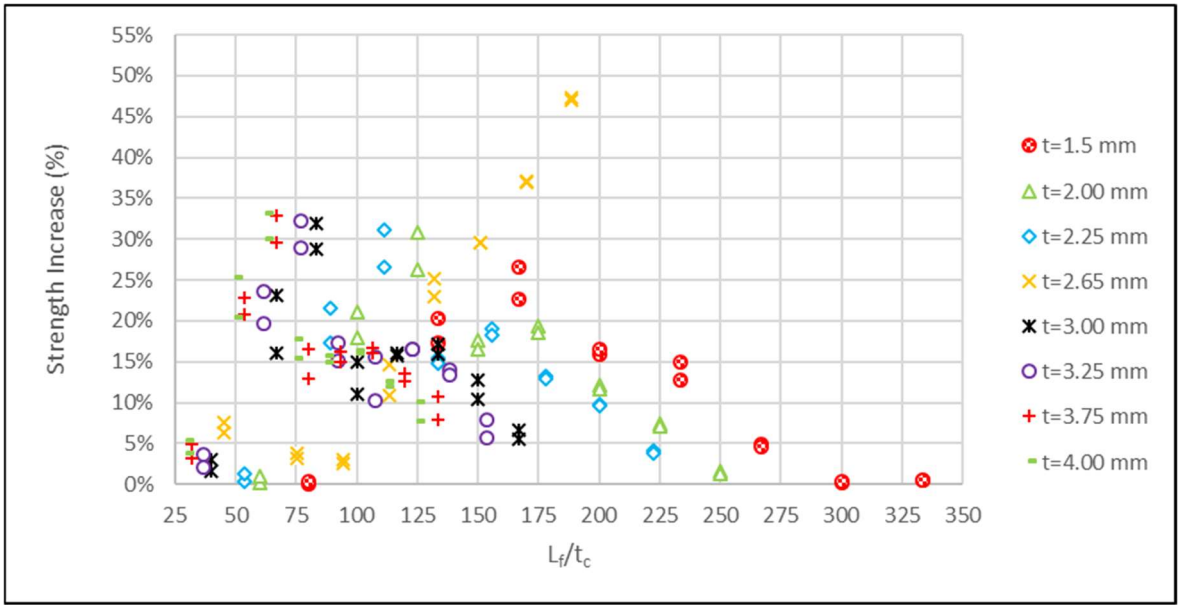

Figure 7. Flexural strength optimization results

Table 4 summarize the general results obtained by the APSO process.

Table 4. Descriptive Statistics over all flexural strength optimization

Descriptive Statistics	M_n (Increase)	b_f/b_w (Modification)	b_s/b_w (Modification)
Mean	14.08%	-34.84%	-35.52%
Standard Deviation	8.61%	14.44%	31.12%
Minimum	0.00%	-55.92%	-72.22%
Maximum	33.20%	22.61%	69.94%

The mean b_f/b_w ratio was 0.27, which corresponds to 27.00% of imposed upper bound (Eq. (14.b)), and mean b_s/b_w was 0.10, which corresponds to lower bound (Eq. (14.a)). Observing mean of both ratios, is noticed a reduction of lips and flange dimension.

Table 5 presents the features of prototype which could not be optimized

Table 5. Not optimizable profile

Profile	f_y (MP_a)	L_f (mm)	t (mm)	M_n (kN.m)	b_w (mm)	b_f (mm)	b_s (mm)	b_f/b_w	b_s/b_w
Standard & Optimized	410.00	120.00	1.50	954.89	50.00	25.00	10.00	0.50	0.20

Table 6 presents the features of prototype with the greatest strength increment.

Table 6. Greatest flexural strength increment

Profile	f_y (MP_a)	L_f (mm)	t (mm)	M_n (kN.m)	b_w (mm)	b_f (mm)	b_s (mm)	b_f/b_w	b_s/b_w
Standard	345.00	250.00	4.00	10781.25	100.00	50.00	25.00	0.50	0.25
Optimized	345.00	250.00	4.00	14360.13	144.00	43.00	10.00	0.30	0.10

Figure 8 presents the shape modification of the prototype with the greatest flexural strength increment.

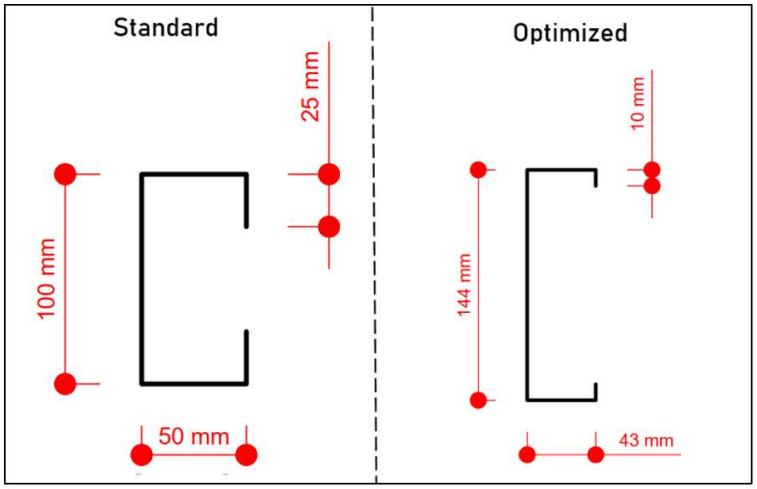

Figure 6. Shape modification of flexural strength optimization

The means of b_f/b_w (-34.84%) and b_f/b_w (-35.52%), indicate a trend of web's length increasing and consequently the rise of inertia moment perpendicular to the web's plane (which is a common solution of flexural strength problems). The results also indicate that profiles manufactured from coils are with widths between 200mm to 300m are more susceptible to optimization. The Fig 7 illustrates general results per coil width.

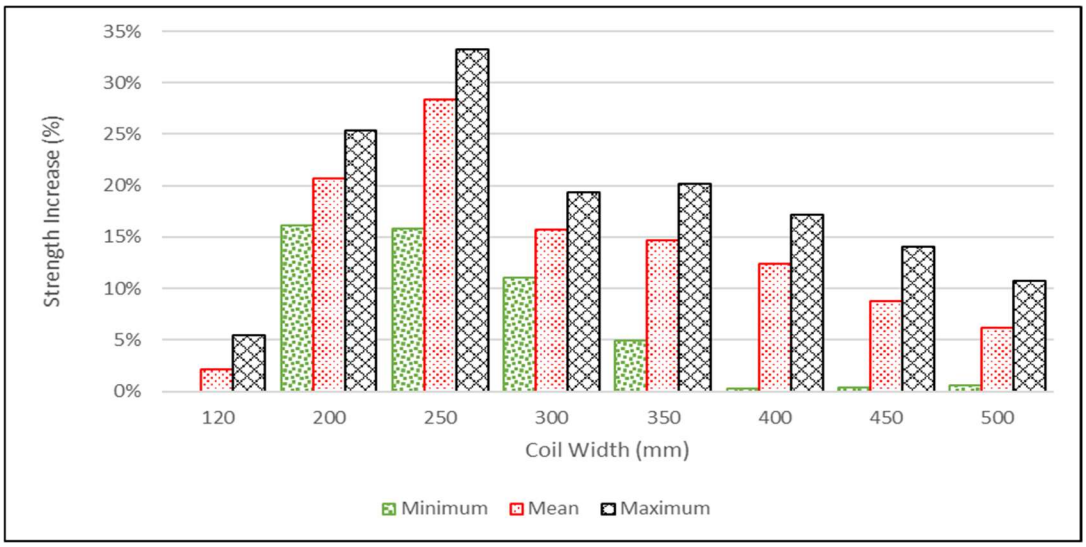

Figure 7. Flexural strength increase per coil width

The results in Figure 8 do not indicate a clear correlation between thickness and the flexural strength increase. Contributing with idea of inertia moment significance's in optimization problems of this nature.

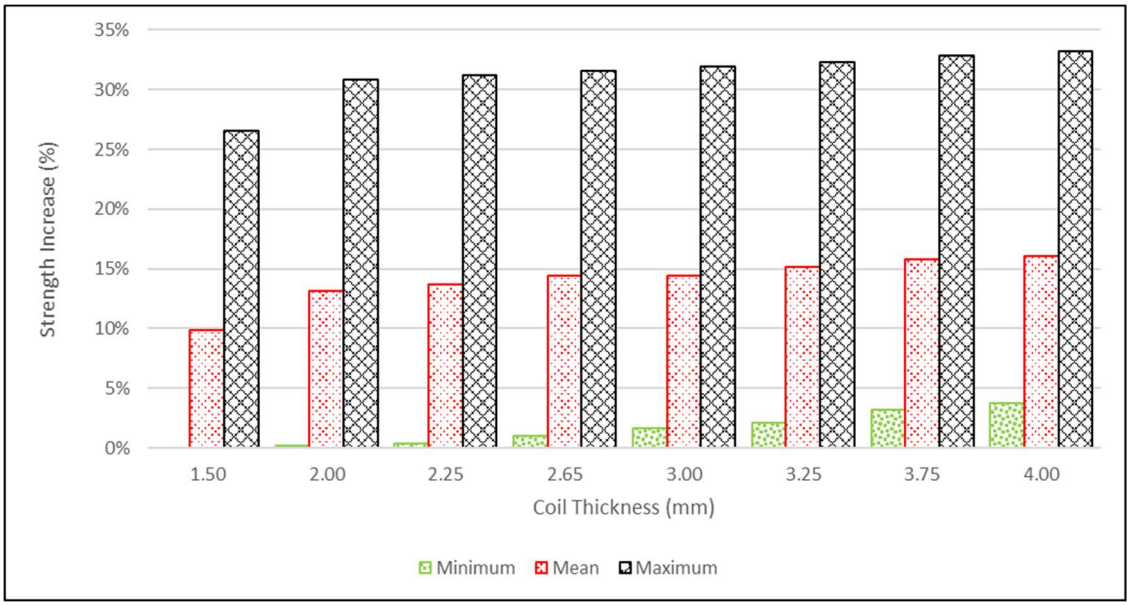

Figure 8. Flexural strength increase per coil thickness

The flexural strength optimization achieved in this work is close obtained by Ye [7], [8], for CFS lipped channel profiles with similar conditions, suggesting that given the methodology applied in this paper, the results are near of best possible.

6 CONCLUSIONS AND FUTURES WORKS

This paper presents a practical method to obtain more efficient CFS lipped channel sections for simply supported beam-columns by optimizing the dimensions of the cross-section and allowing for the addition of double-fold (return) lips. The optimization process is thereby based on the Accelerated Particle Swarm Optimization (APSO) algorithm, while the flexural strength and compressive strength of the sections is determined using the Direct Strength Method (DMS) as implemented in NBR 14762. One hundred twenty-eight different prototypes were considered based on practical considerations. Based on the results of this study, the following conclusions could be drawn:

a. By applying the proposed optimization method to simply supported columns, significant gains in cross-sectional compressive capacity can be achieved: in the examples, the compressive capacity of a CFS cross-section was increased by up to 50% compared to the commercially available section taken as prototype.
b. The APSO can achieve significant gains in cross-sectional bending capacity of simply supported beams: in the examples, the bending capacity of a CFS cross-section was increased by up to 30% compared to the commercially available section taken as a starting point.
c. The strength erosion is a possible consequence of L-D interaction, such as those suggested in the optimized CFS of this work. Thus, case erosion be confirmed in futures analyses, there is demand to create new constrains which avoid the areas strength leak in the feasible region determined by NBR 14762.

The actual work in progress is seeking to explore different cold-formed steel shapes (Hat, Z and Rack, e.g.), variables and constrains for an unsymmetrical optimization of lipped channel shapes

($b_{f\ Superior} \neq b_{f\ Inferior}$,$b_{s\ Superior} \neq b_{s\ Inferior}$,e.g.) ,beam-columns lengths and support conditions. The L-D interaction in optimized CFS is an especial thematic which future works intends to developed, through FEM analysis and experimental study.

7 REFERENCES

[1] Z. Li, J. Leng, J. K. Guest, e B. W. Schafer.Thin-Walled Structures Two-level optimization for a new family of cold-formed steel lipped channel sections against local and distortional buckling. *Thin Walled Structures*, vol. 108, p. 64–74, 2016.

[2] Associação Brasileira de Normas Técnicas, *NBR 14762 -Dimensionamento de estruturas de aço constituídas por perfis formados a frio*, 2010.

[3] European Committee for Standardization.*Design of steel structures-Part 1-1: General rules and rules for buildings*, EN1993-1-1.

[4] W. Ma, J. Becque, I. Hajirasouliha, e J. Ye.Cross-sectional optimization of cold-formed steel channels to Eurocode 3. *Engineering Structures*, vol. 101, p. 641–651, 2015.

[5] P. C. Fourie e A. A. Groenwold.The particle swarm optimization algorithm in size and shape optimization. *Structural and Multidisciplinary Optimization*, vol. 23, nº 4, p. 259–267, 2002.

[6] J. Ye, I. Hajirasouliha, J. Becque, e A. Eslami.Optimum design of cold-formed steel beams using Particle Swarm Optimisation method. *Journal of Constructional Steel Research*, vol. 122, p. 80–93, 2016.

[7] J. Ye, I. Hajirasouliha, J. Becque, e K. Pilakoutas.Development of more efficient cold-formed steel channel sections in bending.*Thin Walled Structures.*, vol. 101, p. 1–13, 2016.

[8] H. Parastesh, I. Hajirasouliha, H. Taji, e A. Bagheri Sabbagh.Shape optimization of cold-formed steel beam-columns with practical and manufacturing constraints.*Journal of Constructional Steel Research*, vol. 155, p. 249–259, 2019.

[9] J. Kennedy e R. Eberhart.Particle Swarm Optimization.*Giornale di Malattie Infettive e Parassitarie*, vol. 46, nº 10, p. 1942–1948, 1994.

[10] K. Gopalakrishnan, *Particle Swarm Optimization in Civil Infrastructure Systems: State-of-the-Art Review*, First Edit. Elsevier Inc., 2013.

[11] J. T. Bryson, X. Jin, e S. K. Agrawal.Optimal Design of Cable-Driven Manipulators Using Particle Swarm Optimization.*Journal of Mechanisms and Robotics*, vol. 8, nº 4, p. 041003, 2015.

[12] X.-S. Yang, "Particle Swarm Optimization", *Nature-Inspired Optimization Algorithms*, First Edit. Elsevier Inc. p. 99–110, 2014.